

1 **Short communication: Field data reveal that the transport probability of clasts in**  
2 **Peruvian and Swiss streams mainly depends on the sorting of the grains**

3  
4 **Running title: transport probability of coarse-grained material**

5  
6 *Fritz Schlunegger, Romain Delunel and Philippos Garefalakis*

7 Institute of Geological Sciences, University of Bern, 3012 Bern, Switzerland

8 +41 31 631 8767, schlunegger@geo.unibe.ch

9  
10 **Abstract**

11 We present field observations from coarse-grained streams in the Swiss Alps and the Peruvian  
12 Andes to explore the controls on the probability of material entrainment. We calculate shear  
13 stress that is expected for a mean annual water discharge, and compare these estimates with  
14 grain-specific critical shear stresses that we use as thresholds. We find that the probability of  
15 material transport largely depends on the sorting of the bed material, expressed by the  $D_{96}/D_{50}$   
16 ratio, and the reach gradient, but not on mean annual discharge. The results of regression  
17 analyses additionally suggest that among these variables, the sorting exerts the largest control on  
18 the transport probability of grains. Furthermore, because the sorting is neither significantly  
19 correlated to reach gradient nor to water discharge, we propose that the granulometric composition  
20 of the material represents an independent, yet important control on the motion of clasts in coarse-  
21 grained streams.

22  
23 **1 Introduction**

24 It has been proposed that the transport of coarse-grained material in mountainous streams occurs  
25 when flow strength, or bed shear stress, exceeds a grain size specific critical shear stress (Miller et  
26 al., 1977; Tucker and Slingerland, 1997; Church, 2006). This has been documented based on flume  
27 experiments (e.g., Meyer-Peter and Müller, 1948; Dietrich et al., 1989; Carling et al., 1992;  
28 Ferguson, 2012; Powell et al., 2016) and field observations (e.g., Paola and Mohring, 1996; Lenzi et  
29 al., 1999; Mueller et al., 2005; Lamb et al., 2008), and related concepts have been employed in  
30 theoretical models (Paola et al., 1992; Tucker and Slingerland, 1997). Whereas flow strength is  
31 mainly a function of discharge, energy gradient and channel width (e.g., Slingerland et al., 1993;  
32 Hancock and Anderson, 2002; Pfeiffer and Finnegan, 2018; Wickert and Schildgen, 2019), the  
33 threshold shear stress itself has been considered to depend on grain specific variables such as grain  
34 size, the arrangement of clasts including hiding and protrusion effects (Carling, 1983; Parker, 1990;  
35 van den Berg and Schlunegger, 2012; Pfeiffer and Finnegan, 2018), but not on the shape of  
36 individual grains (Carling, 1983), or at least this variable plays a minor role only (Komar and Li,  
37 1986). In addition, the threshold shear stress has also been related to the reach gradient (Lamb et al.,  
38 2008; Turowski et al., 2011; Pfeiffer and Finnegan, 2018). Here, we provide field data from coarse-  
39 grained single-thread streams in the Swiss Alps and braided rivers in the Peruvian Andes to

40 illustrate that amongst the various variables, the sorting of the grains exerts the largest control on  
 41 the transport probability. The field sites are located close to water gauging stations so that we have  
 42 good constraints on the streams' discharge in our analyses. We determined the grain size  
 43 distribution of gravel bars at these locations and calculated, within a probabilistic framework  
 44 using Monte-Carlo simulations, the likelihood of sediment transport for a mean annual water  
 45 discharge  $Q_{mean}$ , and for discharge percentiles. We explored whether the related flows are strong  
 46 enough to shift the  $D_{84}$  grain size, which is considered to build the sedimentary framework of  
 47 gravel bars as recent flume experiments have shown (MacKenzie and Eaton, 2017; MacKenzie  
 48 et al., 2018). We thus considered the mobilization of the  $D_{84}$  grain size as a priori condition, and  
 49 thus as a threshold, for a change in the sedimentary arrangement of the target gravels bars.  
 50 The braided character of streams in Peru, however, complicates the calculation of sediment  
 51 transport probabilities mainly because water flows frequently in multiple active channels, and  
 52 channel widths vary over short distances. For these streams, we selected reaches (c. 100 m  
 53 long) where several active braided channels merge to a single one, before branching again. We  
 54 are aware that this could eventually bias the results towards a greater material mobility, mainly  
 55 because flows in single-thread segments are likely to have a greater shear stress than in braided  
 56 reaches where the same water runoff is shared by multiple channels.

57

## 58 **2 Methods and datasets**

### 59 *2.1 Entrainment of bedload material*

60 Sediment mobilization is considered to occur when bed shear stress  $\tau$  exceeds a grain size specific  
 61 threshold  $\tau_c$  (e.g., Paola et al., 1992):

$$62 \quad \tau > \tau_c \quad (1).$$

63 Threshold shear stress  $\tau_c$  for the dislocation of grains with size  $D_x$  (see 2.3.1 for further  
 64 specifications) can be obtained using Shields (1936) criteria  $\phi$  for the entrainment of sediment  
 65 particles:

$$66 \quad \tau_c = \phi(\rho_s - \rho)gD_x \quad (2),$$

67 where  $g$  denotes the gravitational acceleration, and  $\rho_s$  (2700 kg/m<sup>3</sup>) and  $\rho$  the sediment and  
 68 water densities, respectively.

69 Bed shear stress  $\tau$  is computed through (e.g., Slingerland et al., 1993; Tucker and Slingerland,  
 70 1997):

$$71 \quad \tau = \rho gRS \quad (3).$$

72 Here,  $S$  denotes the energy gradient, and  $R$  is the hydraulic radius, which is approximated  
 73 through water depth  $d$  where channel widths  $W > 20d$  (Tucker and Slingerland, 1997), which is  
 74 the case here. The combination of expressions for: (i) the continuity of mass including flow  
 75 velocity  $V$ , channel width  $W$  and water discharge  $Q$ :

$$76 \quad Q = VWd \quad (4);$$

77 (ii) the relationship between flow velocity and channel bed roughness  $n$  (Manning, 1891):

78  $V = \frac{1}{n} d^{2/3} S^{1/2}$  (5);

79 and (iii) an equation for the Manning's roughness number  $n$  (Jarrett, 1984):

80  $n = 0.32 S^{0.38} d^{-1/6}$  (6);

81 yields a relationship where bed shear stress  $\tau$  depends on reach gradient, water discharge and  
82 channel width (Litty et al., 2017):

83  $\tau = 0.54 \rho g \left(\frac{Q}{W}\right)^{0.55} S^{0.935}$  (7).

84 This equation is similar to the expression by Hancock and Anderson (2002), Norton et al.  
85 (2016) and Wickert and Schildgen (2019) with minor differences regarding the exponent on the  
86 channel gradient  $S$  and on the ratio  $Q/W$ . These are mainly based on the different ways of how  
87 bed roughness is considered. Note that this equation does not consider a roughness length scale  
88 (both vertical and horizontal) because we have no constraints on this variable.

89 We explored whether equation (5) could be solved using the Darcy-Weisbach friction factor  $f$   
90 instead of Manning's  $n$ . According to Ferguson (2007), the friction factor  $f$  varies considerably  
91 between shallow- and deep-water flows and depends on grain size  $D_x$  relative to water depth  $d$ ,  
92 and thus on the relative roughness. Ferguson (2007) developed a solution referred to as the  
93 Variable Power Equation (VPE), which accounts for the dependency of  $f$  on the relative  
94 importance of roughness-layer versus skin friction effects and thus on the  $D_x/d$  ratios (see also  
95 Bunte et al., 2013). Calculations where the VPE was employed indeed revealed that roughness-  
96 layer effects have an impact on flow regimes where  $D_{84}/d > 0.2$  (Schlunegger and Garefalakis,  
97 2018), which is likely to be the case in our streams. However, similar to Litty et al. (2016), we are  
98 faced with the problem that we have not sufficient constraints to analytically solve equation (5) with  
99 the VPE. We therefore selected Mannings's  $n$  instead, which allowed us to solve this equation  
100 analytically.

101

## 102 2.2 Monte Carlo simulations

103 Predictions of sediment transport probability are calculated using Monte Carlo simulations  
104 performed within a MATLAB computing environment. We conducted 10'000 simulations, and  
105 the results are reported as the probability (in percent) of  $\tau > \tau_c$  (equation 1). All variables that  
106 are considered for the calculations of both shear and critical shear stress (equations 7 and 2,  
107 respectively) are randomly selected within their possible ranges of variation (Table 1). Except  
108 for the Shields variable  $\phi$  that we consider to follow a uniform distribution between 0.03 and  
109 0.06 (see section 2.3.1 for justification), we infer that all other variables follow normal  
110 distributions, defined by their means and corresponding standard deviations.

111 To ensure that no negative values introduce a bias to these iterations, only strictly positive  
112 values for channel widths and gradients are considered. In the case of water discharge, both null  
113 and positive values are kept for further calculations. Values excluded from the calculations, i.e.  
114 returning negative water discharge or null or negative channel width / slope gradient, yield

115 “NaN” in the resulting vector. For each of the 10’000 iterations  $\tau$  and  $\tau_c$  are compared, which  
116 yields either “1” ( $\tau > \tau_c$ ) or “0” ( $\tau \leq \tau_c$ ). The sediment transport probability is then calculated as the  
117 sum of ones divided by the number of draws, from which the number of “NaN” values was  
118 subtracted before. Note that <2500 “NaN” were obtained for Rio Chico (PRC-ME17), which we  
119 mainly explain by the c. 150% relative standard deviation of the mean annual water discharge  
120 estimated for that river.

121

## 122 2.3 Parameters, datasets, uncertainties and sensitivity analyses

### 123 2.3.1 Shields variable $\phi$ and threshold grain size

124 Assignments of values to  $\phi$  vary and diverge between flume experiments (e.g., Carling et al., 1992;  
125 Ferguson, 2012; Powell et al., 2016) and field observations (Mueller et al., 2005; Lamb et al., 2008).  
126 Here, we considered that at the incipient motion of  $D_{84}$ , the Shields variable  $\phi$  is equally  
127 distributed between 0.03 and 0.06 (Dade and Friend, 1998) during the 10’000 iterations. We also  
128 explored a slope-dependency of  $\phi$  (Lamb et al., 2008; Bunte et al., 2013; Pfeiffer et al., 2017;  
129 Pfeiffer and Finnegan, 2018), where

$$130 \phi = 0.15S^{0.25} \quad (8).$$

131 However, applying this slope-dependent characterization of  $\phi$  did not change our overall  
132 finding that the transport probability is dependent on the sorting of the material (Supplement  
133 S1). In the same context, Turowski et al. (2011) reported a larger variation in the threshold  
134 conditions for the mobilization of clasts than those employed here. However, their streams have  
135 energy gradients between 0.06 and 0.1, with the consequence that some of the material is entrained  
136 during torrential floods. The related conditions thus differ to those of the much flatter streams  
137 (reach gradients < 0.02), which we explored in this paper. Finally, we did not explicitly include a  
138 grain-size specific hiding (e.g., equation A8 in Pfeiffer and Finnegan, 2018) or a protrusion function  
139 (e.g., Carling, 1983; Sear, 1996; van der Berg and Schlunegger, 2012) in our analysis, but we  
140 suggest that the selected range between 0.03 and 0.06 considers most of the complexities and  
141 scatters of  $\phi$ -values that are related to the hiding of small clasts and the protrusion of large  
142 constituents (Buffington et al., 1992; Buffington and Montgomery, 1997; Kirchner et al., 1990;  
143 Johnston et al., 1998). In summary, we infer that the selection of uniformly distributed  $\phi$ -values  
144 between 0.03 and 0.06 does account for the large variability of  $\phi$ -values that are commonly  
145 encountered in experiments and field surveys where energy gradients range between 0.001 and  
146 0.02, which is the case here.

147 We consider that the most important critical shear stress is that required to move  $D_{84}$ , rather than  
148 any other grain size percentile. We acknowledge that other authors preferentially selected the  $D_{50}$   
149 grain size as a threshold to quantify the minimum flow strengths  $\tau_c$  to entrain the bed material (e.g.,  
150 Paola and Mohrig, 1996; Pfeiffer and Finnegan, 2018; Chen et al., 2018). The selection of  $D_{50}$   
151 results in a lower threshold and a greater transport probability than the employment of  $D_{84}$ . However,  
152 among the various grain sizes,  $D_{84}$  has been considered to best characterize the sedimentary

153 framework of a gravel bar (Howard, 1980; Hey and Thorne, 1986; Grant et al., 1990), and more  
154 recent experiments have also shown that  $D_{84}$  better characterizes the channel form stability than  $D_{50}$   
155 (MacKenzie et al., 2018). Accordingly, flows that dislocate the  $D_{84}$  grain size are considered strong  
156 enough to alter the gravel bar architecture. We therefore followed the recommendation by  
157 MacKenzie et al. (2018) and selected the  $D_{84}$  grain size to quantify the threshold conditions in  
158 equation (2).

159

### 160 2.3.2 Grain size data

161 We collected grain size data from streams where water discharge has been monitored during the  
162 past decades. These are the Kander, Lütschine, Rhein, Sarine, Simme, Sitter and Thur Rivers in  
163 the Swiss Alps (Fig. 1a). The target gravel bars are situated close to a water gauging station. At  
164 these sites, 5 to 6 digital photographs were taken with a Canon EOS PR. The photos covered  
165 the entire lengths of these bars. A meter stick was placed on the ground and photographed  
166 together with the grains. Grain sizes were then measured with the Wolman (1954) method using  
167 the free software package ImageJ 1.52n (<https://imagej.nih.gov>). Following Wolman (1954), we  
168 used intersecting points of a grid to randomly select the grains to measure. A digital grid of  
169 20x20 cm was calibrated with the meter stick on each photo. The size of the grid was selected  
170 so that the spacing between intersecting points was larger than the  $b$ -axis of most of the largest  
171 clasts (Table 1, Supplement S2). The grid was then placed on the photograph with its origin at  
172 the lower left corner of the photo. The intermediate or  $b$ -axis of approximately 250 – 300 grains  
173 (c. 50 grains per photo; Supplement S2) underneath a grid point was measured for each gravel  
174 bar. In this context, we inferred that the shortest ( $c$ -axis) was vertically oriented, and that the  
175 photos displayed the  $a$ - and  $b$ -axis only. In cases where more than half of the grain appeared to  
176 be buried, the neighboring grain was measured instead. In the few cases where the same grain  
177 lay beneath several grid points, then the grain was only measured once. Only grains larger than  
178 a few millimeters (>4-5 mm, depending on the quality and resolution of the photos) could be  
179 measured. While the limitation to precisely measure the finest-grained particles potentially  
180 biases the determination of  $D_{50}$ , it will not influence the measurements of the  $D_{84}$  and  $D_{96}$  grain  
181 sizes, as the comparison between sieving and measuring of grains with the Wolman (1954)  
182 method has disclosed (Watkins et al., 2020). In addition, as will be shown below, the  
183 consideration of the  $D_{96}/D_{84}$  instead of the  $D_{96}/D_{50}$  ratios yields a similar positive relationship to  
184 the mobility of grains. We complemented the grain size data sets with published information on  
185 the  $D_{50}$ ,  $D_{84}$  and  $D_{96}$  grain size (Litty and Schlunegger, 2017; Litty et al., 2017) for further  
186 streams in Switzerland (6 additional rivers) and Peru (21 sites) (Figs. 1a and 1b; Table 1). For a  
187 few streams in Switzerland, Hauser (2018) presented  $D_{84}$  grain size data from the same gravel  
188 bars as Litty and Schlunegger (2017), but the photo was taken one year later and possibly from  
189 a different site. For these 5 locations, we took the arithmetic mean of both surveys (Table 1,  
190 data marked with three asterisks). All authors used the same approach upon collecting grain  
191 size data, which justifies the combination of the new with the published datasets.

192 We finally assigned an uncertainty of 20% to the  $D_{84}$  threshold grain size, which considers the  
193 variability of  $D_{84}$  within a gravel bar as the analysis of the intra-bar variation of  $D_{84}$  for selected  
194 gravel bars in Switzerland shows (Supplement S2). The assignment of a 20% uncertainty to the  
195  $D_{84}$  threshold grain size also considers a possible bias that could be related to the grain size  
196 measuring technique (e.g., sieving in the field versus grain size measurements using the  
197 Wolman method; Watkins et al., 2020). However, it is likely to underestimate the temporal  
198 variability in the grain size data. Indeed, a repeated measurement on some gravel bars in  
199 Switzerland has revealed that up to twofold differences in grain size could be possible (Hauser,  
200 2018).

201

### 202 2.3.3 *Water discharge data*

203 The Federal Office for the Environment (FOEN) of Switzerland has measured the runoff values  
204 of Swiss streams over several decades. We employed the mean annual discharge values over 20  
205 years for these streams (Supplement S3) and calculated one standard deviation thereof (see  
206 Table 1). For the Peruvian streams, we used the mean annual water discharge values  $Q_{mean}$   
207 reported by Litty et al. (2017) and Reber et al. (2017). These authors obtained the mean annual  
208 water discharge (Table 1) through a combination of hydrological data reported by the Sistema  
209 Nacional de Información de Recursos Hídricos and the TRMM-V6.3B43.2 precipitation  
210 database (Huffman et al., 2007). They also considered the intra-annual runoff variability as one  
211 standard deviation from  $Q_{mean}$  to account for the strong seasonality in runoff for the Peruvian  
212 streams, which we employed in this paper. For the Peruvian streams, the assigned uncertainties  
213 to  $Q_{mean}$  are therefore significantly larger than for the Swiss rivers (Table 1). A re-assessment of the  
214 inter-annual variability of water discharge for those streams in Peru where the gauging sites are  
215 close to the grain size sampling location (distance of a few kilometres) yields a one standard  
216 deviation of c. 50%, which is still much larger than for the Swiss rivers (Supplement S3). We  
217 therefore run sensitivity tests where we considered scenarios with different relative values for 1 $\sigma$   
218 standard deviations of  $Q_{mean}$ .

219 We additionally ran sensitivity tests to explore how the mobility probability changes if discharge  
220 quantiles instead of  $Q_{mean}$  are considered (Supplement S4). We ran a series of Monte Carlo  
221 simulations for various discharge quantiles and then calculated the resulting probability of sediment  
222 mobilization for each of these quantiles. We then multiplied the occurrence probability of each  
223 discharge quantiles (listed by the Swiss authorities and calculated for the Peruvian streams based on  
224 4 to 98-years equivalent daily records) with the corresponding transport probability and summed the  
225 values. This integration provides an alternative estimate of transport probability (Supplement S4).

226

### 227 2.3.4 *Channel width data*

228 For the Swiss streams, channel widths and gradients (Table 1) were measured on orthophotos  
229 and LiDAR DEMs with a 2-m resolution provided by Swisstopo. From this database, gradients

230 were measured over a reach of c. 250 to 500 m. All selected Swiss rivers are single-thread  
231 streams following the classification scheme of Eaton et al. (2010), and flows are constrained by  
232 artificial banks where channel widths are constant over several kilometers. For these streams,  
233 we therefore measured the cross-sectional widths between the channel banks, similar to Litty  
234 and Schlunegger (2017).

235 We complemented this information with channel width (wetted perimeter) and energy gradient  
236 data for 21 Peruvian streams that were collected by Litty et al. (2017) in the field and on  
237 orthophotos taken between March and June. This period also corresponds to the season when  
238 the digital photos for the grain size analyses were made (Mai 2015). We acknowledge that  
239 widths of active channels in Peru vary greatly on an annual basis because of the strong  
240 seasonality of discharge (see above and large intra-annual variability of discharge in Table 1).  
241 We therefore considered scenarios where channel widths are twice as large as those reported in  
242 Table 1.

243 The uncertainties on reach gradient and channel width largely depend on the resolution of the digital  
244 elevation models underlying the orthophotos (2-m LiDAR DEM for Switzerland, and 30-m ASTER  
245 DEM for Peru). It is not possible to precisely determine the uncertainties on the gradient values.  
246 Nevertheless, we anticipate that these will be smaller for the Swiss rivers than for the Peruvian  
247 streams mainly because of the higher resolution of the DEM. We ran sensitivity models where we  
248 explored how the probability of material transport changes in the Swiss rivers for various  
249 uncertainties on channel widths, energy gradients and mean annual discharge values.

250

### 251 **3 Results**

#### 252 *3.1 Grain size data, critical and bed shear stress, and transport probability*

253 The grain sizes range from 8 mm to 70 mm for  $D_{50}$ , 29 mm to 128 mm for  $D_{84}$ , and 52 mm to 263  
254 mm for  $D_{96}$ . The smallest and largest  $D_{50}$  values were determined for the Maggia and Rhein Rivers  
255 in the Swiss Alps, respectively (Table 1). The grain sizes in the Swiss rivers also reveal the largest  
256 spread where the ratio between the  $D_{96}$  and  $D_{50}$  grain size ranges between 2.2 (Saraine) and 17.7  
257 (Maggia Losone I), while the corresponding ratios in the Peruvian streams are between 2.1 (PRC-  
258 ME9) and 5.8 (PRC-ME17). In the Swiss Alps, the critical shear stress values  $\tau_c$  (median) for  
259 entraining the  $D_{84}$  grain size range from c. 20 Pa (Emme River) to c. 90 Pa (Rhein and Simme  
260 Rivers). In the Peruvian Andes, the largest critical shear values are <80 Pa (PRC-ME39). The shear  
261 stress values related to the mean annual water discharge  $Q_{mean}$  range from c. 15 Pa to 100 Pa in the  
262 Alps and from 20 Pa to >400 Pa in the Andes. Considering the strength of a mean annual flow and  
263 the  $D_{84}$  grain size as threshold, the probability of sediment transport occurrence in the Peruvian  
264 Andes and in the Swiss Alps comprises the full range between 0% and 100%.

265 Rivers that are not affected by recurrent high magnitude events (e.g., debris flows) and where  
266 the grain size distribution is not perturbed by lateral material supply are expected to display a self-  
267 similar grain size distribution (Whittaker et al., 2011; D'Arcy et al., 2017; Harries et al., 2018),

268 characterized by a linear relationship between the  $D_{84}/D_{50}$  and  $D_{96}/D_{50}$  ratios. In case of the Maggia  
269 River, the largest grains are oversized if  $D_{50}$  and the grain size distribution of the other streams are  
270 considered as reference (Fig. 2A). This could reflect a response to the supply of coarse-grained  
271 material by a tributary stream where the confluence is <1 km upstream of the Maggia sites.  
272 Alternatively, and possibly more likely, it reflects the response to the high magnitude floods in this  
273 stream (Brönnimann et al., 2018) that could explain why the largest grains tend to be oversized. In  
274 particular, while the ratio between the last and first quantiles of discharge is <150 in the Swiss  
275 streams on the northern side of the Alps, the ratio is 860 in the Maggia River. Such ratios are not  
276 rare in Peru. However, the Peruvian streams appear to have adapted to such large discharge  
277 variability through their network of braided channels that are not confined by artificial banks along  
278 most of the streams. In either case, because the grains in the Maggia River have a different size  
279 composition than the other streams (Figure 2A), we excluded the Maggia data from further analyses.  
280 From this dataset, we then explored whether  $D_{84}$  depends on the sorting of the grains ( $D_{96}/D_{50}$  ratio),  
281 but a possible negative correlation between these variables is very weak ( $R^2=0.2$ ) with a p-value of  
282 0.011 (Figure 2B).

283

### 284 3.2 *Correlations between channel metrics, water discharge, material sorting and transport* 285 *probability*

286 The probability of sediment transport occurrence correlates positively with the reach gradient ( $R^2 =$   
287  $0.46$ , p-value =  $0.016$  for Swiss rivers, and  $R^2 = 0.34$ , p-value =  $0.0056$  for streams in Peru; Fig. 3A).  
288 For the Peruvian rivers, the probability of occurrence also scales negatively with channel width ( $R^2$   
289 =  $0.37$ , p-value =  $0.0033$ ; Fig. 3B) and critical shear stress  $\tau_c$  ( $R^2 = 0.48$ , p-value =  $0.00047$ ; Fig.  
290 3D), which itself depends on the threshold grain size  $D_{84}$ . No significant correlations are found  
291 between the transport probability and mean annual water discharge for the Swiss and Peruvian  
292 rivers (Fig. 3C).

293 Notably, the probability of material transport correlates positively and linearly with the  $D_{96}/D_{50}$  ratio  
294 (Fig. 4A). The observed relationship appears stronger for the Swiss rivers ( $R^2 = 0.76$ ), than for the  
295 Peruvian streams ( $R^2 = 0.36$ ), and both correlations are significant with p-values of  $0.00022$  and  
296  $0.0041$ , respectively. These correlations suggest that poorer-sorted bed material, here expressed by a  
297 high  $D_{96}/D_{50}$  ratio, has a greater transport probability than better-sorted sediments. If the normalized  
298 residuals are plotted against the sorting, then they do not show any specific and significant patterns,  
299 and therefore appear independent of the sorting (Fig. 4B). This suggests that the inferred linear  
300 relationships between the transport probability and the  $D_{96}/D_{50}$  ratio are statistically robust.  
301 Although Fig. 4A implies that the regression for the Swiss rivers (slope:  $0.16\pm 0.06$ ; intercept: -  
302  $0.34\pm 0.31$ ) differs from that of the Peruvian streams (slope:  $0.18\pm 0.11$ ; intercept:  $-0.02\pm 0.46$ ), the  
303 regression parameters do not significantly differ when considering them within their 95%  
304 confidence intervals. In addition, sites with larger values of  $D_{96}/D_{50}$  tend to be associated with  
305 smaller values of  $D_{84}$  (albeit with a weak correlation), but as noted earlier the influence of  $D_{84}$  on the



306 critical shear stress is not sufficient to explain the observed relationship between mobility and  
307  $D_{96}/D_{50}$  in the Swiss streams.

308 Because the sorting itself could potentially depend on channel metrics and water discharge, we  
309 explored possible correlations between these variables. We find that the  $D_{96}/D_{50}$  ratio negatively  
310 correlates with channel widths for Peruvian streams ( $R^2 = 0.20$ , p-value = 0.040), but not with any  
311 of the other variables in both mountain ranges (e.g. reach gradient, mean annual discharge and  
312 discharge variability; see Supplement S5). In the same sense, the positive relationship between the  
313  $D_{96}/D_{50}$  ratio and the reach gradient in the Swiss Rivers ( $R^2 = 0.23$ ) is statistically not significant (p-  
314 value = 0.12). As mentioned above, the  $D_{96}/D_{50}$  ratio negatively correlates with  $D_{84}$ , but the  
315 correlation is poor and explains 20% of the observations only (Figure 2B).

316

### 317 3.4 Discharge quantiles, uncertainties on reach slopes, and channel widths

318 The use of discharge quantiles yields sediment transport probabilities that are positively and linearly  
319 correlated with the transport probability estimated with  $Q_{mean}$  (Figure S4 in Supplement). In  
320 addition, the correlations are very similar between the Swiss (slope:  $0.74 \pm 0.02$ ; intercept:  
321  $0.05 \pm 0.01$ ) and Peruvian streams (slope:  $0.73 \pm 0.19$ ; intercept:  $0.03 \pm 0.14$ ). The mean annual  
322 discharge estimates  $Q_{mean}$  are likely biased by infrequent, but large magnitude floods, which could  
323 explain the 25% larger transport probabilities if  $Q_{mean}$  is used as reference discharge.

324 The assignments of different uncertainties on reach gradients, channel widths and discharge has no  
325 major influence on the inferred relationships between transport probability and sorting (Supplement  
326 S6, S7). For the Peruvian streams, however, assignments of twofold larger values to channel widths  
327 will decrease the transport probability for a given sorting by c. 10-15%, consistent with Fig. 3B and  
328 Supplement 5 that illustrate negative correlations between channel width,  $D_{96}/D_{50}$  ratio and transport  
329 probability. The inferred linear relationship between both variables, however, will remain  
330 (Supplement S7).

331

## 332 4 Discussion

### 333 4.1 Controls of channel metrics on the transport probability

334 Our analysis documents a slope dependency of sediment transport probability for the Swiss and  
335 Peruvian streams. Such a relationship has been documented before for mountainous rivers in the  
336 USA (Torizzo and Pitlick, 2004; Pfeiffer and Finnegan, 2018) and for other sites including the  
337 Alps (Van den Berg and Schlunegger, 2012). Pfeiffer and Finnegan (2018) reported transport  
338 probabilities, at conditions of an annual flow, that range between 8% and nearly 100% for the West  
339 Coast in the USA, 1% and 12% for the Rocky Mountains, and <10% for the Appalachian  
340 Mountains. These estimates are generally lower than the probabilities reported here. This most  
341 likely reflects the effect of the low channel gradients of the US streams that are c. three times flatter  
342 than the rivers analyzed here (Table 1). These differences thus emphasize the controls of the reach  
343 gradient on the entrainment probability of coarse-grained bed material.

344 The regression analysis also documents that channel widths and critical shear stress have an

345 influence on the transport probability of clasts. This is particularly the case for the braided streams  
346 in Peru where wider channels and greater critical shear stresses tend to lower the transport  
347 probability (Fig. 3B, 3D). Since braided streams dynamically adjust their channel widths to changes  
348 in the caliber and the rates of the supplied material (Church, 2006), a dependency of transport  
349 probability on channel width and grain-size specific threshold (including  $D_{84}$ ) was expected. The  
350 absence of corresponding relationships in the Swiss streams is probably due to the managed  
351 geometry of these streams where artificial banks constrain the channel widths over tens of  
352 kilometers.

353

#### 354 4.2 Controls of material sorting on the transport probability

355 Interestingly, our regression analysis of the variables disclosed a positive correlation between the  
356  $D_{96}/D_{50}$  ratio of the bed material and the transport probability. This relationship maintains if  
357 transport probabilities are calculated based on discharge quantiles (Supplement S4), and if larger  
358 channel width and discharge variability particularly for Peruvian streams are considered  
359 (Supplement S7). Such a dependency will also remain if critical shear stress is calculated using a  
360 different grain size percentile. This is because grain size  $D_x$  linearly propagates into the equation (2)  
361 and thus into the probability of  $\tau > \tau_c$ . Therefore, although the resulting probabilities will adjust  
362 according to the threshold grain size, the relationships between the  $D_{96}/D_{50}$  ratio and the  
363 mobilization probability will not change. Furthermore, because of the linear relationship between  
364 the  $D_{84}/D_{50}$  and  $D_{96}/D_{50}$  ratios (Fig. 2), the same dependency of transport probability on the sorting  
365 will also emerge if the  $D_{96}/D_{84}$  ratios are used. This suggests that the sorting of the bed material has  
366 a measurable impact on the mobility of gravel bars and thus on the frequency of sediment  
367 mobilization irrespective of the selection of a threshold grain size. In addition, there appears to be a  
368 feedback where a poorer sorting (large  $D_{96}/D_{50}$  ratio) tends to be associated with a lower  $D_{84}$  (Figure  
369 2), which additionally increases the sediment transport probability. We note that while the data is  
370 relatively scarce and scattered (i.e., the same transport probability for a c. twofold difference in the  
371  $D_{96}/D_{50}$  ratio), the relationships observed between the probability of transport occurrence and the  
372 degree of material sorting are significant with p-values  $\ll 0.05$ . Finally, for a given  $D_{96}/D_{50}$  ratio, the  
373 probability of material transport tends to be greater in the Peruvian than in the Swiss rivers (Fig.  
374 4A). We tentatively explain the apparent small divergence in the transport probability between both  
375 settings (i.e. regression parameters overlap within their 95% confidence interval) by the differences  
376 in the flow patterns (braided versus single-thread artificial channels).

377

#### 378 4.3 Controls on the sorting of the bed material

379 None of the possible variables such as channel reach gradient, mean water discharge and discharge  
380 variability are significantly correlated with the bed material sorting (Supplement S5). Exceptions  
381 are the Peruvian streams where wider channels tend to be associated with a better sorting (i.e., lower  
382  $D_{96}/D_{50}$  ratio). We lack further quantitative information to properly interpret these patterns, but it

383 appears that material sorting represents an additional, yet independent variable that influences the  
384 probability of transport, at least for the sites we have investigated in this paper. Because the sorting  
385 of the bed material in the analyzed streams appears not to strongly depend on the hydrological  
386 conditions at the reach scale, it could possibly reflect an inherited supply signal from further  
387 upstream (Pfeiffer et al., 2017). Indeed, detailed grain size analyses along fluvial gorges in the  
388 Swiss Alps have shown that the hillslope-derived supply of large volumes of sediment perturbs the  
389 granulometric composition of the bed material (van den Berg and Schlunegger, 2012; Bekaddour et  
390 al., 2013). Using the results of flume and numerical experiments, Jerolmack and Paola (2010)  
391 suggested that these source signals are likely to be shredded during sediment transport as a  
392 consequence of what they considered as ubiquitous thresholds in sediment transport systems.  
393 However, based on a detailed analysis of downstream fining trends in alluvial fan deposits,  
394 Whittaker et al. (2011), D'Arcy et al. (2016) and Brook et al. (2018) proposed that primary source  
395 signals of grain size compositions are likely to propagate farther downstream in a self-similar way.  
396 Accordingly, the original grain-size sorting of the supplied material could be maintained although a  
397 general fining of the sediments along the sedimentary routing system would be observed. This idea  
398 could offer an explanation why the  $D_{96}/D_{50}$  ratios are to large extents independent from other  
399 variables. It also points to the importance of sediment supply not only on controlling the bankfull  
400 hydraulic geometry of channels (Pfeiffer et al., 2017), but also on the sorting of the material. Finally,  
401 a supply control could possibly explain why sorting appears to vary with  $D_{84}$ , albeit with a poor  
402 correlation, where a better sorting tends to be associated with larger  $D_{84}$ .

403

#### 404 4.4 *Relative importance of sorting versus gradient on the transport probability*

405 Because gradient and sorting are independent variables and since the transport probability  
406 depends linearly on both variables, then the transport probability can be described as a linear,  
407 but weighted combination of gradient and sorting. We therefore assess whether the transport  
408 probability ( $Tp$ ) in both the Swiss ( $i=1$ ) and the Peruvian ( $i=2$ ) rivers can be predicted using a  
409 multiple linear regression:  $Tp_i = \alpha_i S_n + \beta_i G_n + \delta_i$ , where  $S_n$  and  $G_n$  are the sorting and  
410 gradient normalized to their respective maximum, and  $\alpha$ ,  $\beta$  and  $\delta$  are the regression parameters.  
411 We decided to normalize both the sorting and gradient to their maximum values so that both  
412 variables vary on a similar [0-1] range, and the inferred linear coefficients  $\alpha$ ,  $\beta$  and  $\delta$  can be  
413 directly compared between the Swiss and the Peruvian rivers. The model outputs show that  
414 when sorting and gradient are combined, then the predictions of the transport probability in  
415 both the Swiss ( $R^2 = 0.85$ ,  $p = 2.24e-4$ ) and the Peruvian ( $R^2 = 0.61$ ,  $p = 1.9e-4$ ) rivers are  
416 significantly improved compared to simple linear regressions. The results also reveal that the  
417 relative importance of sorting on the transport probability is greater ( $\alpha$  is  $1.22 \pm 0.26$  for the  
418 Swiss streams,  $1.46 \pm 0.41$  for the Peruvian streams) than the relative controls of reach gradient  
419 ( $\beta$  is  $0.62 \pm 0.27$  for the Swiss streams,  $0.67 \pm 0.20$  for the Peruvian rivers). The comparison of  
420 the estimated factors thus suggests that the relative importance of sorting on the transport

421 probability could be twice as large as the controls of gradient, although our estimation is  
422 associated with large uncertainties ( $2.0\pm 1.0$  in Switzerland,  $2.2\pm 0.9$  in Peru). Interestingly, we  
423 also note that the apparent greater probability of transport in the Peruvian rivers, as we infer  
424 based on all simple linear regressions reported in Figures 3 and 4, remains with our multiple  
425 linear regression analysis ( $\delta$  is  $-0.42\pm 0.12$  for the Swiss streams,  $-0.28\pm 0.19$  for the Peruvian  
426 streams; Figure 5). Again, this suggests that an additional component (intrinsic geomorphic  
427 setting such e.g., as braided vs. single-thread) may contribute to the observed higher probability  
428 of sediment transport in the Peruvian rivers than in the Swiss ones. The search for an answer to  
429 this questions, however, is beyond the scope of this paper and would require additional  
430 research.

431

### 432 **Conclusions**

433 We confirm the results of previous research that the transport probability of coarse-grained material  
434 in mountainous streams largely depends on the reach gradient. We also find a positive correlation  
435 between the  $D_{96}/D_{50}$  ratio of the bed material and the transport probability where a poorer sorting of  
436 the material results in a larger probability of material entrainment. Despite the large scatter in the  
437 dataset, this relationship is statistically significant with p-values  $\ll 0.05$ , which suggests that the  
438 sorting of coarse-grained bed sediments has a measurable impact on the mobility of the bedload  
439 material. Regression analyses additionally reveal that sorting exerts a greater control on the  
440 transport probability than reach gradient. Furthermore, the lack of a significant correlation between  
441 reach gradient and sorting implies that both variables are largely independent from each other, at  
442 least for the investigated rivers in Switzerland and Peru. We therefore propose that the sorting of the  
443 bed material represents an additional, yet important variable that influences the mobility of material  
444 on gravel bars. Finally, we identify two main open questions that we cannot resolve with our dataset.  
445 First, Figure 5 illustrates that 15% of the transport probability observations in Switzerland and 40%  
446 of the data in Peru cannot be fully explained by a combination of sorting and reach gradient, and  
447 interpretations thereof most likely require the consideration of the anthropogenic management of  
448 the streams (braided and free flow in Peru versus engineered single-thread channels in Switzerland).  
449 Second, we have not identified a significant correlation between the sorting and the other variables  
450 such as reach gradient, water discharge and discharge variability. This led us to propose that  
451 material supply need to be included in the discussion as well. Furthermore, the critical shear stress,  
452 through its dependency on  $D_{84}$ , is also a function of the sorting (albeit with a poor correlation,  
453 Figure 2B). This could invoke a possible feedback where a poorer sorting tends to be associated  
454 with lower  $D_{84}$  and thus with a lower critical shear stress, which further promotes the mobility of  
455 grains. We don't have the required data to fully address these latter two questions and suggest that it  
456 could serve as a topic in future research.

457

458 Figure 1

459 A) Map showing the sites where grain size data has been measured in the Swiss Alps. The research  
460 sites are close to water gauging stations; B) map showing locations for which grain size and water  
461 discharge data is available in Peru (Litty et al., 2017).

462

463 Figure 2

464 A) Relationship between ratio of the  $D_{96}/D_{50}$  and  $D_{84}/D_{50}$ , implying that the  $D_{96}$  grain sizes of the  
465 Maggia gravel bars are too large if the  $D_{50}$  is taken as reference and if the other gravel bars are  
466 considered. B) Relationships between  $D_{84}$  and sorting, expressed by the  $D_{96}/D_{50}$  ratio. The Maggia  
467 data is not considered in this figure. However, the negative correlation between these variables is  
468 weak.

469

470 Figure 3

471 Relationships between transport probability and (A) reach gradient, (B) channel width, (C) mean  
472 annual discharge and (D) critical shear stress that depends on the  $D_{84}$ .

473

474 Figure 4

475 A) Relationships between the probability of sediment transport occurrence and the  $D_{96}/D_{50}$  ratio,  
476 which we use as proxy for the sorting of the gravel bar, in the Swiss and Peruvian rivers. B)  
477 Normalized residuals that are plotted against the sorting. The normalized residuals do not show  
478 any specific and significant patterns.

479

480 Figure 5

481 Transport probability for the Swiss and Peruvian rivers plotted as a function of the combined  
482 response to gradient and sorting. Blue diamonds correspond to the Swiss rivers while grey  
483 circles are Peruvian ones. Both best multiple linear regression fits (solid line) and their 95%  
484 confidence intervals (dashed curves) are presented. Note that the variables on the axis are  
485 adjusted as a result of projecting the multiple linear regression models onto a bivariate plot.

486

487 Table 1

488 Channel morphometry (width and gradient), grain size and water discharge measured at the research  
489 sites. The table also shows the results of the various calculations (critical shear stress  $\tau_c$ , shear stress  
490  $\tau$  of a flow with a mean annual runoff  $Q_{mean}$  and probability of sediment transport occurrence related  
491 to this flow).

492

#### 493 **Data availability**

494 All data that have been used in this paper are listed in Table 1 and in the Supplement.

495

#### 496 **Author contributions**

497 FS and RD designed the study. RD conducted the Monte Carlo Simulation. PG provided the grain  
498 size data in the Supplement. FS wrote the paper with input from RD and PG. All authors discussed  
499 the article.

500

#### 501 **Competing interests**

502 The authors declare that they have no conflict of interest.

503

#### 504 **Acknowledgements**

505 The Federal Office for the Environment (FOEN) is kindly acknowledged for providing runoff data  
506 for the Swiss streams. This research was supported by SNF (No. 155892). The constructive  
507 comments by Georgios Maniatis, two anonymous reviewers and the handling editor (Rebecca  
508 Hodge) are kindly acknowledged and significantly improved the science of this paper.

509

#### 510 **References**

- 511 Bekaddour, T., Schlunegger, F., Attal, M., and Norton, K.P., Lateral sediment sources and  
512 knickzones as controls on spatio-temporal variations of sediment transport in an Alpine  
513 river, *Sedimentology*, 60, 342-357, 2013.
- 514 Bunte, K., Abt, S.R., Swingle, K.W., Cenderelli, D.A., and Schneider, M.: Critical Shields values in  
515 coarse-bedded steep streams, *Water Res. Res.*, 49, 7427-7447, 2013.
- 516 Brönnimann, S., et al.: 1968 – das Hochwasser, das die Schweiz veränderte. Ursachen, Folgen und  
517 Lehren für die Zukunft, *Geographica Bernensia*, G94, 52 p., 2018
- 518 Buffington, J., Dietrich, W.E., and Kirchner, J.W., Friction angle measurements on a naturally  
519 formed gravel streambed: Implications for critical boundary shear stress, *Water Res.*  
520 *Res.*, 28, 411-425, 1992.
- 521 Buffington, J. M. and Montgomery, D. R.: A systematic analysis of eight decades of incipient  
522 motion studies, with special reference to gravel-bedded rivers, *Water Resour. Res.*, 33,  
523 1993-2029, 1997.
- 524 Carling, P.A., Threshold of coarse sediment transport in broad and narrow natural streams, *Earth*  
525 *Surf. Process. Landf.*, 8, 1-18, 1983.
- 526 Carling, P. A., Kelsey, A., and Glaister, M. S.: Effect of bed roughness, particle shape and  
527 orientation on initial motion criteria, in: *Dynamics of gravel-bed rivers*, edited by: Billi, P.,  
528 Hey, R. D., Throne, C. R., and Tacconi, P., 23–39, John Wiley and Sons, Ltd., Chichester,  
529 1992.
- 530 Chen, C., Guerit, L., Foreman, B.Z., Hassenruck-Gudipati, H.J., Adatte, T., Honegger, L., Perret,  
531 M., Sluijs, A., Castelltort, S., Estimating regional flood discharge during Palaeocene-  
532 Eocene global warming, *Sci. Rep.*, 8, 13391.
- 533 Church, M.: Bed material transport and the morphology of alluvial river channels, *Ann. Rev. Earth*  
534 *Planet. Sci.*, 34, 325-354, 2006.
- 535 D’Arcy, M., Whittaker, A.C., and Roda-Bolduda, D.C.: Measuring alluvial fan sensitivity to past

536 climate changes using a self-similarity approach to grain-size fining, Death Valley,  
537 California, *Sedimentology*, 64, 388-424, 2017.

538 Dade, B. and Friend, P.F.: Grain-size, sediment-transport regime, and channel slope in alluvial  
539 rivers, *J. Geol.*, 106, 661-676, 1988.

540 Dietrich, W.E., Kirchner, J.W., Hiroshi, I., and Iseya, F.: Sediment supply and the development of  
541 the coarse surface layer in gravel-bedded rivers, *Nature*, 340, 215-217, 1989.

542 Eaton, B.C., Moore, R.D., and Giles, T.R.: Forest fire, bank strength and channel instability: the  
543 'unusual' response of Fishtrap Creek, British Columbia, *Earth Surf. Process. Landf.*, 35,  
544 1167-1183, 2010.

545 Ferguson, R., Flow resistance equations for gravel- and boulder- bed streams. *Water Resour. Res.*,  
546 43, W05427, 2007.

547 Ferguson, R.: River channel slope, flow resistance, and gravel entrainment thresholds, *Water  
548 Resources Research*, 48, W05517, 2012.

549 Grant, G. E., Swanson, F. J., and Wolman, M. G.: Pattern and origin of stepped-bed morphology in  
550 high gradient streams, western Cascades, Oregon, *GSA Bull.*, 102, 340-352, 1990.

551 Hancock, G.S., and Anderson, B.S.: Numerical modeling of fluvial strath-terrace formation in  
552 response to oscillating climate, *GSA Bull.*, 9, 1131-1142, 2002.

553 Harries, R.M., Kirstein, L.A., Whittaker, A.C., Attal, M., Peralta, S., and Brooke, S.: Evidence for  
554 self-similar bedload transport on Andean alluvial fans, Iglesia, basin, South Central  
555 Argentina, *J. Geophys. Res. - Earth Surface*, 123, 2292-2315, 2018.

556 Hauser, R.: Abhängigkeit von Korngrößen und Flussformen in den Schweizer Alpen, Unpubl.  
557 Ms thesis, Univ. Bern, Bern, Switzerland, 64 p., 2018.

558 Hey, R. D. and Thorne, C. R.: Stable channels with mobile gravel beds, *J. Hydrol. Eng.*, 112, 671-  
559 689, 1986.

560 Howard, A. D.: Threshold in river regimes, in: *Thresholds in geomorphology*, edited by: Coates,  
561 D.R, and Vitek, J.D., Allen and Unwin, Boston, MA, 227-258, 1980.

562 Huffman, G. J., Adler, R. F., Bolvin, D. T., Gu, G., Nelkin, E. J., Bowman, K. P., and Wolff, D. B.:  
563 The TRMM multi-satellite precipitation analysis: Quasi-global, multi-year, combined-  
564 sensor precipitation estimates at fine scale, *J. Hydromet.*, 8, 38-55, 2007.

565 Jarrett, R. D.: Hydraulics of high-gradient streams, *J. Hydraul. Eng.*, 110, 1519-1939, 1984.

566 Johnston, C.E., Andrews, E.D., and Pitlick, J., In situ determination of particle friction angles  
567 of fluvial gravels, *Water Resour. Res.*, 34, 2017-2030, 1998.

568 Kirchner, J.W., Dietrich, W.E., Iseya, F., and Ikeda, H.: The variability of critical shear stress,  
569 friction angle, and grain protrusion in water-worked sediments, *Sedimentology*, 37, 647-  
570 672, 1990.

571 Komar, P.D., and Li, Z.: Pivoting analyses of the selective entrainment of sediments by shape and  
572 size with application to gravel threshold, *Sedimentology*, 33, 425-436, 1986.

573 Lenzi, M.A., Luca Mao, L., and Comiti, F.: When does bedload transport begin in steep boulder-  
574 bed streams? *Hydrol. Process.*, 20, 3517-3533, 2006.

575 Lamb, M. P., Dietrich, W. E., and Venditti, J. G.: Is the critical Shields stress for incipient sediment  
576 motion dependent on channel bed slope? *J. Geophys. Res.*, 113, F02008, 2008.

577 Litty, C., Duller, R., Schlunegger, F., Paleohydraulic reconstruction of a 40 ka-old terrace sequence  
578 implies that water discharge was larger than today, *Earth Surf. Proc. Landf.*, 41, 884-898,  
579 2016.

580 Litty, C. and Schlunegger, F.: Controls on pebbles' size and shape in streams of the Swiss Alps, *J.*  
581 *Geol.*, 125, 101-112, 2017.

582 Litty, C., Schlunegger, F., and Viveen, W.: Possible threshold controls on sediment grain properties  
583 of Peruvian coastal river basins, *Earth Surf. Dyn.*, 5, 571-583, 2017.

584 MacKenzie, L. and Eaton, B.C.: Large grains matter: constraining bed stability and  
585 morphodynamics during two nearly identical experiments, *Earth Surf. Proc. Landf.*,  
586 42, 1287-1295, 2017.

587 MacKenzie, L., Eaton, B.C. and Church, M.: Breaking from the average: Why large grains  
588 matter in gravel-bed streams. *Earth Surf. Proc. Landf.*, 43, 3190-3196, 2018.

589 Manning, R.: On the flow of water in open channels and pipes, *Trans. Inst. Civil Eng. Ireland*, 20,  
590 161–207, 1891.

591 Meyer-Peter, E., and Müller, R., Formulas for bedload transport, *Proceedings of the 2<sup>nd</sup> meeting of*  
592 *the Int. Assoc. Hydraul. Struct. Res.*, Stockholm, Sweden. Appendix 2, 39–64, 1948.

593 Miller, M.C., McCave, I.N., and Komar, P.D., Threshold of sediment motion under unidirectional  
594 currents, *Sedimentology*, 24, 507-527, 1977.

595 Mueller, E. R., Pitlick, J., and Nelson, J. M.: Variation in the reference Shields stress for bed load  
596 transport in gravel- bed streams and rivers, *Water Res. Res.*, 41, W04006, 2005.

597 Norton, K.P., Schlunegger, F., and Litty, C.: On the potential for regolith control of fluvial terrace  
598 formation in semi-arid escarpments, *Earth Surf. Dyn.*, 4, 147-157, 2016.

599 Paola, C., Heller, P.L., and Angevine, C.: The large-scale dynamics of grain size variation in  
600 alluvial basins, 1: Theory, *Basin Res.*, 4, 73-90, 1992.

601 Paola, C. and Mohring, D.: Palaeohydraulics revisited: palaeoslope estimation in coarse-grained  
602 braided rivers, *Basin Res.*, 8, 243-254, 1996.

603 Parker, G., Surface-based bedload transport relation for gravel rivers, *J. Hydraul. Res.*, 28, 417-436,

604 Pfeiffer, A.M., Finnegan, N.J., and Willenbring, J.K., Sediment supply controls equilibrium  
605 channel geometry in gravel rivers, *Proc. Natl. Acad. Sci. U.S.A.*, 114, 3346-3351,  
606 2017.

607 Pfeiffer, A.M., and Finnegan, N.J.: Regional variation in gravel riverbed mobility, controlled by  
608 hydrological regime and sediment supply, *Geophys. Res. Lett.*, 45, 3097-3106, 2018.

609 Powell, M. D., Ockleford, A., Rice, S. P., Hillier, J. K., Nguyen, T., Reid, I., Tate, N. J., and  
610 Ackerley, D.: Structural properties of mobile armors formed at different flow strengths in  
611 gravel-bed rivers, *J. Geophys. Res. – Earth Surface*, 121, 1494-1515, 2016.

612 Reber, R., Delunel, R., Schlunegger, F., Litty, C., Madella, A., Akcar, N., and Christl, M.:



613 Environmental controls on  $^{10}\text{Be}$ -based catchment-averaged denudation rates along the  
614 western margin of the Peruvian Andes, *Terra Nova*, 29, 282-293, 2017.

615 Turowski, J.M., Badoux, A., and Rickenmann, D., Start and end of bedload transport in gravel-bed  
616 streams, *Geophys. Res. Lett.*, 38, L04401, 2011.

617 Schlunegger, F., and Garefalakis, P., Clast imbrication in coarse-grained mountain streams and  
618 stratigraphic archives as indicator of deposition in upper flow regime conditions, *Earth*  
619 *Surf. Dyn.*, 6, 743-761.

620 Sear, D.A., Sediment transport processes in pool-riffle sequences, *Earth Surf. Process. Landf.*, 21,  
621 241-262, 1996.

622 Shields A.: Anwendung der Ahnlichkeitsmechanik und der Turbulenzforschung auf die  
623 Geschiebebewegung, *Mitt. Preuss. Versuch. Wasserbau Schiffbau*, 26 p., Berlin, 1936.

624 Slingerland, R., Harbaugh, J., and Furlong, K., *Simulating clastic sedimentary basins*. Prentice-Hall,  
625 Englewood Cliffs, New Jersey, 220 p., 1993.

626 Torizzo, M., and Pitlick, J.: Magnitude-frequency of bed load transport in mountain streams in  
627 Colorado, *J. Hydrol.*, 290, 137-151.

628 Tucker, G., and Slingerland, R.: Drainage basin responses to climate change, *Water Res. Res.*, 33,  
629 2031-2047, 1997.

630 Van den Berg, F., and Schlunegger, F., Alluvial cover dynamics in response to floods of various  
631 magnitudes: The effect of the release of glaciogenic material in a Swiss Alpine catchment,  
632 *Geomorphology*, 141-142, 112-133, 2012.

633 Watkins, S., Whittaker, A.C., Bell, R.E., Brooke, S.A.S., Ganti, V., Gawthrope, R.L., McNeill, L.C.,  
634 and Nixon, C.W.: Straight from the source's mouth: Controls on field-constrained  
635 sediment export across the entire active Corinth rift, central Greece, *Basin Res.*, in press.  
636 Doi: 10.1111/bre.12444.

637 Whittaker, A.C., Duller, R.A., Springett, J., Smithells, R.A., Whitchurch, A.L., and Allen, P.A.:  
638 Decoding downstream trends in stratigraphic grain size as a function of tectonic subsidence  
639 and sediment supply, *GSA Bull.*, 123, 1363-1382, 2011.

640 Wickert, A.D., and Schildgen, T.F.: Long-profile evolution of transport-limited gravel-bed rivers,  
641 *Earth Surf. Dyn.*, 7, 17-43, 2019.

642 Wolman, M. G.: A method of sampling coarse riverbed material, *Eos Trans AGU*, 35, 951-956,  
643 1954.

644  
645  
646

Id	River	Site coordinates Latitude (DD WGS84)	Site coordinates Longitude (DD WGS84)	Channel width along reach (m)	Reach gradient (m/m)	Omean: Mean annual water discharge (m3/s)	Standard deviation of Omean (m3/s)**	D50 (m)	D84 (m)	D96 (m)	D96/D50	D84/D50	Critical Shear (median) (Pa)	Critical Shear (16th%) (Pa)	Critical Shear (84th%) (Pa)	Shear stress in response to Omean (median) (Pa)	Shear stress in response to Omean (16th%) (Pa)	Shear stress in response to Omean (84th%) (Pa)	Transport probability for Omean and the D84 as threshold
1	Emme*	46.98	7.75	30	0.007	11.9	2.5	0.009	0.029	0.052	5.8	3.2	21	15	29	30	23	39	81%
2	Landquart*	46.98	9.61	32	0.018	24.1	5.1	0.025	0.083***	0.135	5.4	3.3	60	42	82	102	79	130	90%
3	Waldermme Littau*	47.07	8.28	27	0.011	15.5	2.8	0.009	0.050***	0.084	9.3	5.5	36	26	50	55	42	69	85%
4	Reuss*	46.88	8.62	48	0.007	42.9	4.7	0.009	0.032***	0.064	7.2	4.1	27	19	37	48	38	60	93%
5	Maggia Losone II*	46.17	8.77	84	0.005	22.7	10.8	0.011	0.046***	0.127	11.3	4.1	33	23	46	19	12	26	11%
6	Maggia Losone I*	46.17	8.77	22	0.005	22.7	10.8	0.008	0.033***	0.140	17.7	4.1	24	17	33	39	26	53	83%
7	Rhein	47.01	9.30	92	0.002	167.5	24.5	0.070	0.128	0.169	2.4	1.8	92	65	127	26	20	32	0%
8	Sarine	46.36	7.05	24	0.004	21.0	3.9	0.049	0.080	0.108	2.2	1.6	58	41	80	27	21	35	4%
9	Lötschine	46.38	7.53	32	0.007	19.0	1.7	0.061	0.111	0.153	2.5	1.8	80	56	110	39	31	49	4%
10	Thur	47.30	9.12	52	0.002	37.9	6.8	0.024	0.045	0.069	2.9	1.8	32	23	45	13	10	17	2%
11	Simme	46.39	7.27	15	0.014	12.0	1.8	0.062	0.119	0.263	4.2	1.9	86	61	118	87	68	109	51%
12	Sitter	47.24	9.19	26	0.005	10.2	1.6	0.028	0.064	0.094	3.3	2.2	46	33	64	24	19	30	6%
13	Kander	46.39	7.40	26	0.009	20.0	2.3	0.054	0.116	0.193	3.6	2.1	84	59	115	58	46	72	19%
14	Sense*	46.89	7.35	24	0.005	8.7	1.7	0.024	0.060	0.096	4.0	2.5	43	31	60	22	17	28	6%
15	PRC-ME1#	-18.12	-70.33	6	0.015	3.4	0.8	0.023	0.062	0.100	4.3	2.7	45	32	62	76	58	97	89%
16	PRC-ME3#	-17.82	-70.51	6	0.013	4.0	5.0	0.025	0.055	0.110	4.4	2.2	40	28	55	83	46	126	86%
17	PRC-ME5#	-17.29	-70.99	7	0.018	3.4	1.0	0.026	0.051	0.078	3.0	2.0	37	26	51	82	61	107	96%
18	PRC-ME6#	-17.03	-71.69	26	0.051****	38.1	37.8	0.015	0.036	0.075	5.0	2.4	26	18	36	432	244	643	100%****
19	PRC-ME802#	-16.34	-72.13	15	0.019	30.1	21.7	0.020	0.060	0.100	5.0	3.0	43	31	60	193	116	278	98%
20	PRC-ME7#	-16.51	-72.64	100	0.005	68.4	52.7	0.052	0.087	0.120	2.3	1.7	63	44	86	31	18	45	8%
21	PRC-ME9#	-16.42	-73.12	70	0.004	91.1	82.2	0.048	0.068	0.100	2.1	1.4	49	35	68	37	21	54	29%
22	PRC-ME1402#	-15.85	-74.26	3	0.014	20.4	29.9	0.013	0.030	0.060	4.6	2.3	22	15	30	336	182	510	100%
23	PRC-ME15#	-15.63	-74.64	23	0.003	12.1	16.7	0.029	0.064	0.096	3.3	2.2	46	33	64	19	10	29	5%
24	PRC-ME16#	-13.73	-75.89	20	0.013	13.6	17.8	0.030	0.066	0.130	4.3	2.2	48	34	66	85	47	129	80%
25	PRC-ME17#	-13.47	-76.14	5	0.010	10.1	14.8	0.013	0.038	0.076	5.8	2.9	28	19	38	126	68	191	97%
26	PRC-ME19#	-13.12	-76.39	60	0.010	25.4	25.9	0.020	0.046	0.088	4.4	2.3	33	23	46	49	28	72	72%
27	PRC-ME20#	-12.67	-76.65	22	0.008	8.2	9.8	0.016	0.048	0.088	5.5	3.0	35	25	48	38	21	57	55%
28	PRC-ME22#	-12.25	-76.89	5	0.022	3.7	4.3	0.030	0.050	0.088	2.9	1.7	36	26	50	141	78	212	96%
29	PRC-ME39#	-11.79	-76.99	40	0.018	4.9	5.1	0.053	0.105	0.150	2.8	2.0	76	54	104	42	24	63	13%
30	PRC-ME23#	-11.61	-77.24	20	0.010	8.9	7.8	0.055	0.083	0.120	2.2	1.5	60	42	82	48	27	70	32%
31	PRC-ME25#	-11.07	-77.59	5	0.012	3.8	4.6	0.028	0.077	0.130	4.6	2.8	56	39	77	82	45	124	72%
32	PAT-ME4	-10.72	-77.77	30	0.014	30.9	24.3	0.018	0.036	0.060	3.3	2.0	26	18	36	102	60	148	97%
33	PRC-ME38#	-10.07	-78.16	15	0.004	9.8	12.7	0.017	0.034	0.052	3.1	2.0	25	17	34	28	15	42	56%
34	PRC-ME27#	-8.97	-78.62	40	0.005	96.1	67.7	0.020	0.054	0.090	4.5	2.7	39	27	54	61	37	87	77%
35	PRC-ME30#	-7.32	-79.48	40	0.007	25.4	27.7	0.029	0.063	0.100	3.4	2.2	45	32	63	44	24	65	46%

*Italic*=Swiss Rivers, plain=Peruvian Rivers

Water discharge data from the Swiss Rivers is taken from the Swiss Federal Office for the Environment (FOEN: www.hydrodaten.admin.ch). Reported values represent discharges monitored over the period 1990-2011; Except for the Rhein (1977-1990).

Water discharge and drainage basin size data from the Peruvian Rivers is taken from Reber et al. (2017) and Litty et al. (2017)

#The grain size data from the Peruvian streams is taken from Litty et al. (2017)

\*The grain size data, channel width and gradient data from the Emme, Landquart, Reuss, Maggia and Sense Rivers is taken from Litty and Schlunegger (2017)

\*\*While standard deviation on annual water flow represents inter-annual variance for Switzerland, it represents intra-annual ones in Peru.

\*\*\*Mean values of measurement results by Hauser (2017) and Litty and Schlunegger (2017)

\*\*\*\*The results are possibly biased by an error on the slope, which appears too steep; the consideration of a flatter slope (0.013) still yields 99%

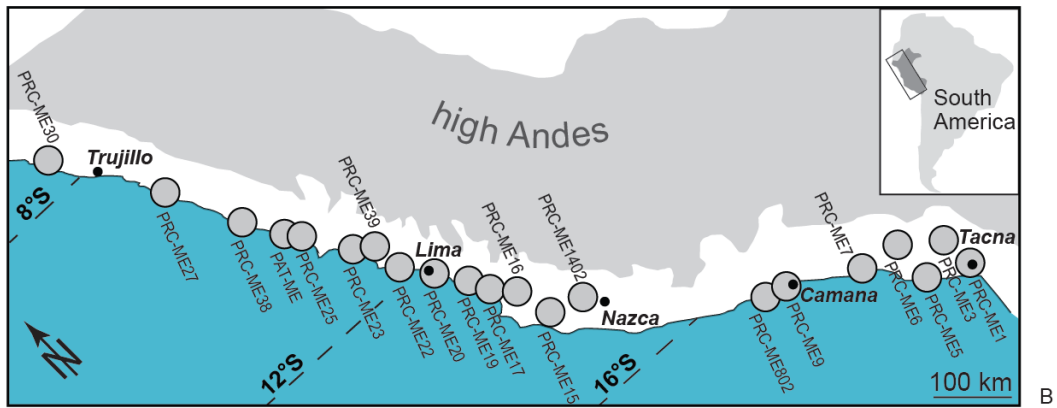
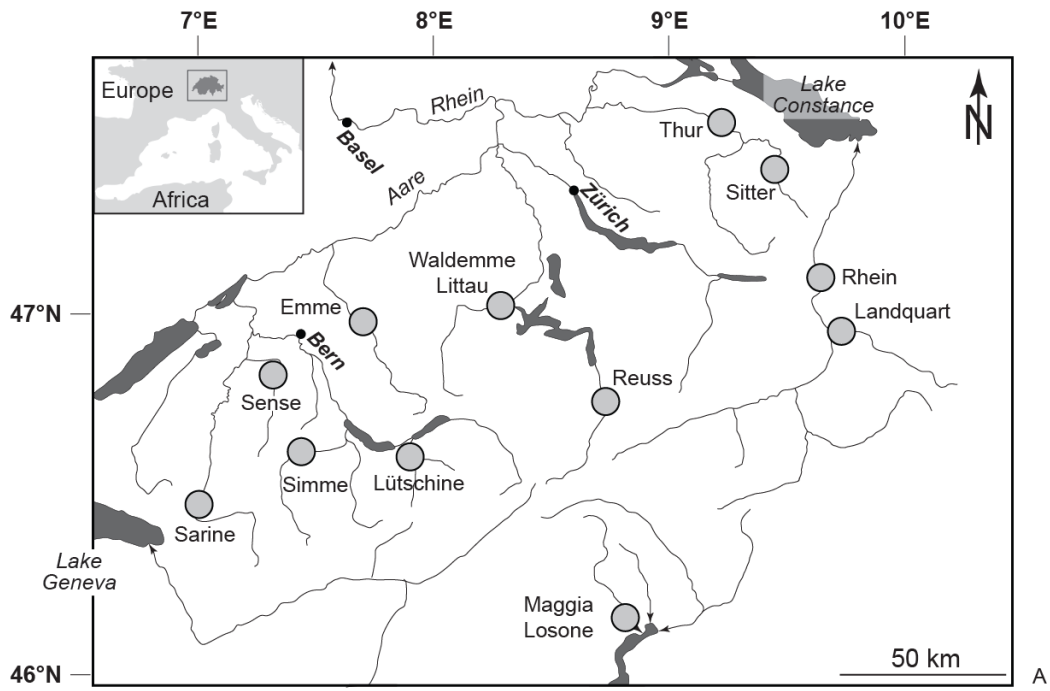


Figure 1

650

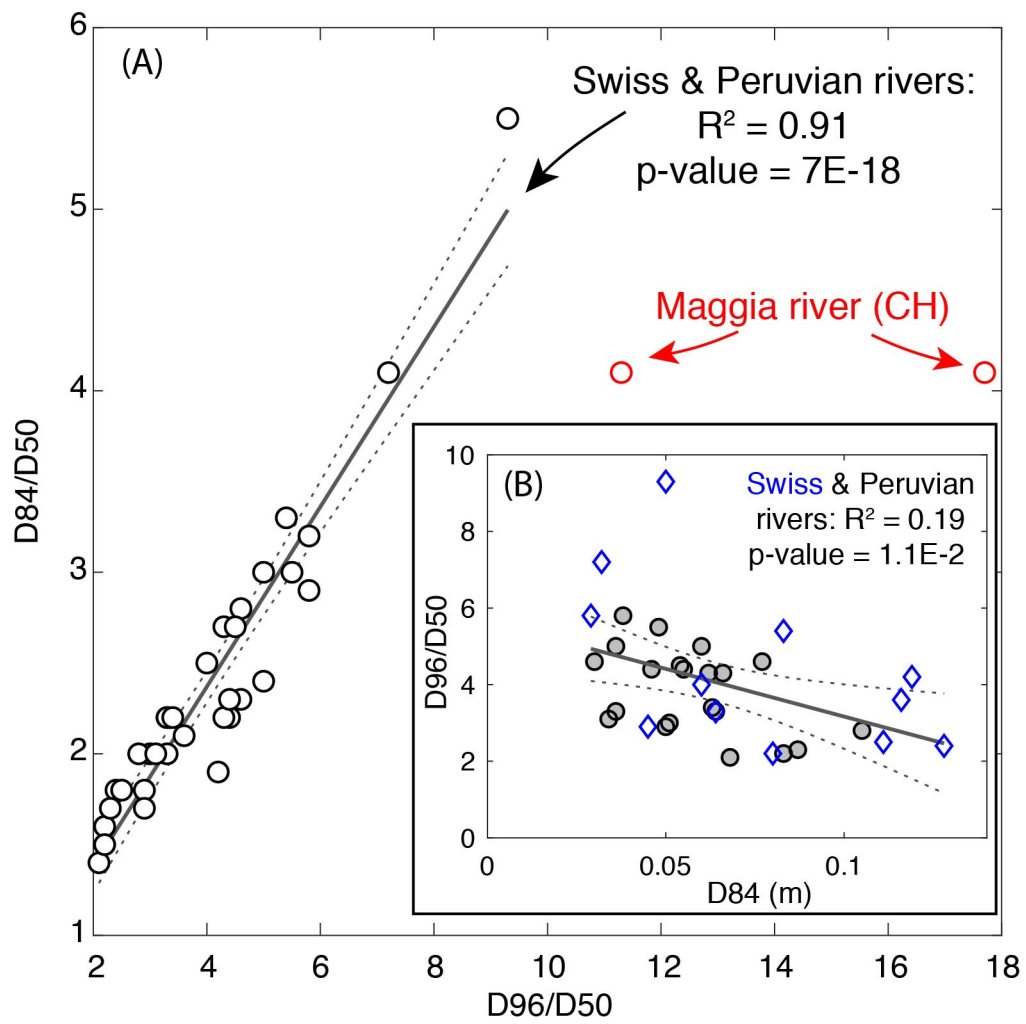
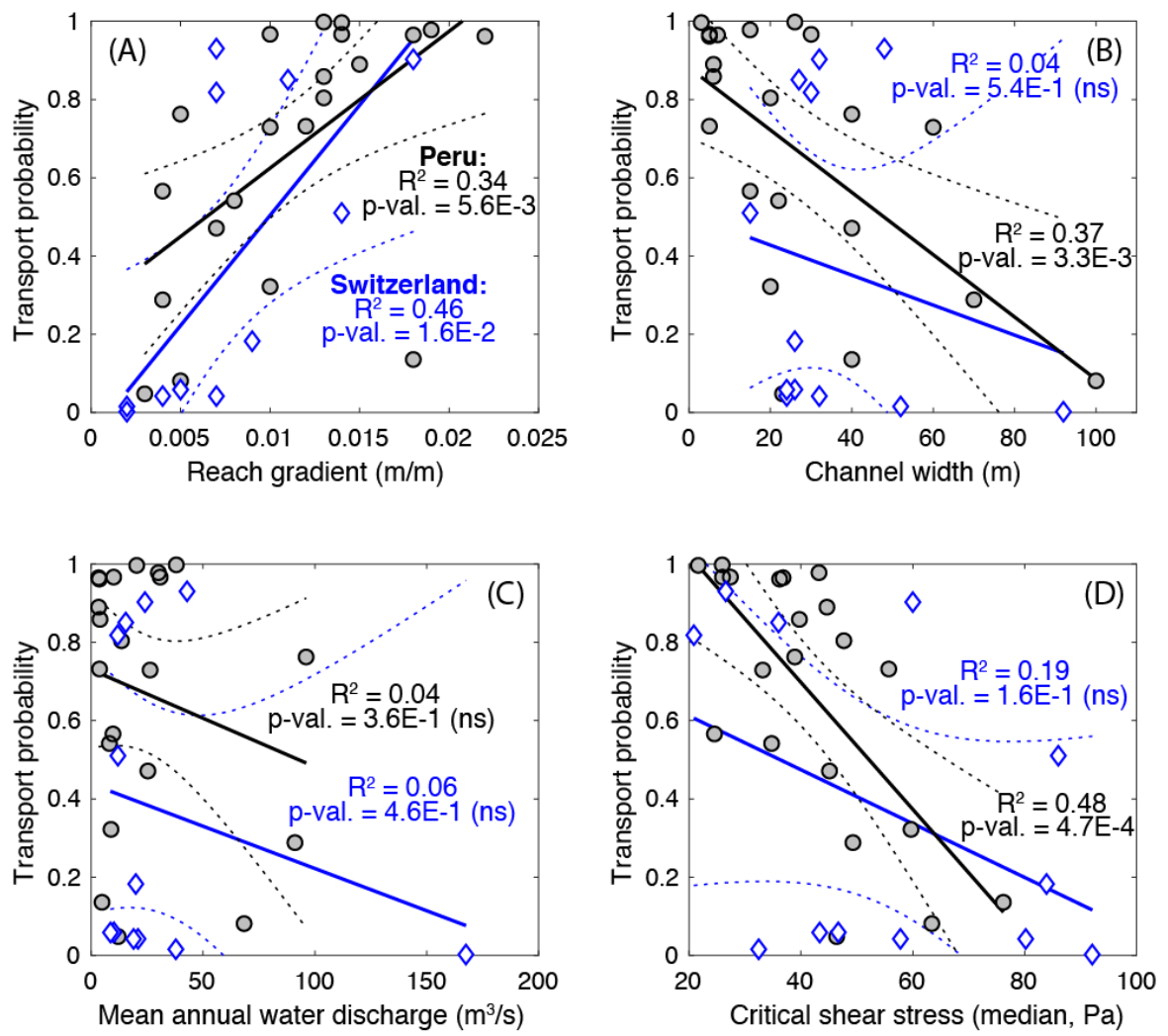


Figure 2

651  
 652  
 653  
 654  
 655  
 656



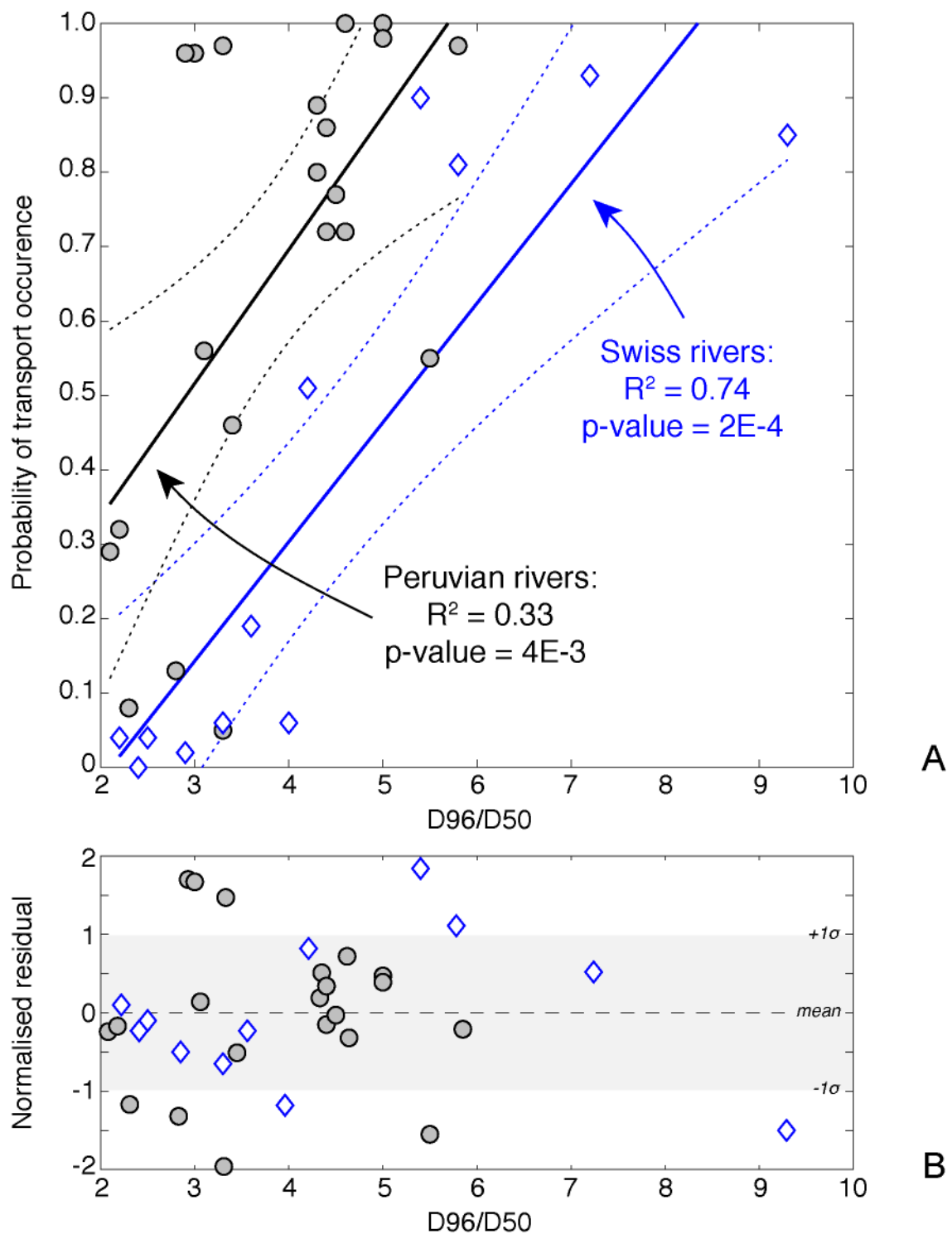


Figure 4

658

659

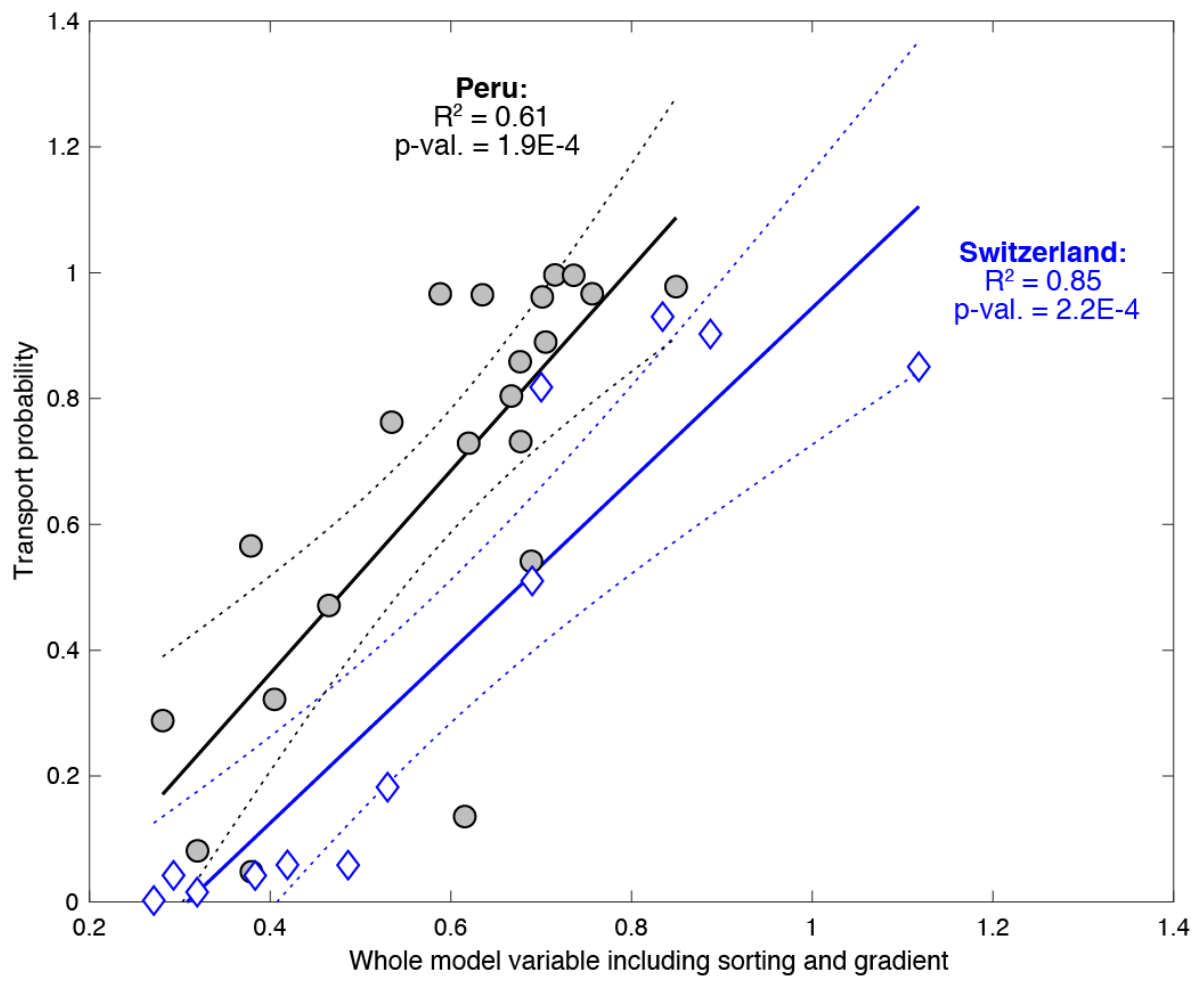


Figure 5